Radiomic Feature Spatially Characterizes the Transition of Normal Lung Parenchyma to Small Airways Disease in COPD

Alexander J. Bell, PhD[a]; Sundaresh Ram, PhD[a,b*]; Wassim W. Labaki, MD[c]; Benjamin A. Hoff, PhD[a]; Jennifer M. Wang, MD[c]; Susan Murray, PhD[d]; Ella A. Kazerooni, MD[a]; Stefanie Galban, PhD[a]; David A. Lynch, MB Bch[e]; Stephen M. Humphries, PhD[e]; Fernando J. Martinez, PhD[f]; Charles R. Hatt, PhD[g]; MeiLan K. Han, MD[c]; Craig J. Galban, PhD[a*]

[a] Department of Radiology, University of Michigan, Ann Arbor, MI, United States

[b] Department of Biomedical Engineering, University of Michigan, Ann Arbor, MI, United States

[c] Department of Internal Medicine, Division of Pulmonary and Critical Care Medicine, University of Michigan, Ann Arbor, MI, United States

[d] School of Public Health, University of Michigan, Ann Arbor, MI, United States

[e] Department of Radiology, National Jewish Health, Denver, CO, United States

[f] Weill Cornell Medical College, New York, NY, United States

[g] Imbio, LLC, Minneapolis, MN, United States

Corresponding author

Sundaresh Ram, PhD
Department of Radiology
University of Michigan
Biomedical Science Research Building, Room A504
109 Zina Pitcher Place
Ann Arbor, MI 48109-2200
Email: sundarer@umich.edu
Phone: 734-764-8726

Short Title: CT Readout improves SAD Quantification

Abstract

Purpose: Small airways disease (SAD), a major cause of airflow obstruction in COPD patients, has been identified as a precursor to emphysema. Nevertheless, there is a lack of clinical techniques that can quantify the progression of SAD. We aim to determine if our Parametric Response Mapping (PRM) method to quantify SAD offers insight into lung progression from healthy to emphysema.

Materials and Methods: PRM metrics quantifying normal lung (PRM^{Norm}) and functional SAD (PRM^{fSAD}) were generated from CT scans collected as part of the COPDGene study (n=8956). Volume density (V) and Euler-Poincaré Characteristic (χ) maps, measures of extent and coalescence of pocket formations, respectively, were determined for both PRM^{Norm} and PRM^{fSAD}. Association with COPD severity, emphysema, and spirometric measures were assessed via multivariable regression models.

Results: Across all GOLD, we observed a strong linear correlation between χ^{fSAD} and χ^{Norm} (ρ =-0.745, p<0.001). Values of χ^{fSAD} and χ^{Norm} were found to flip signs in unison between GOLD 2 and 4, demonstrating an inversion in parenchymal topology. For subjects with COPD, multivariable analysis showed that both χ^{fSAD} (β of 0.106, p<0.001) and V^{fSAD} (β of 0.065, p=0.004) were independently associated with FEV_1% predicted. V and χ measures for PRM^{fSAD} and PRM^{Norm} were independently associated with the amount of emphysema.

Conclusions: We demonstrated that χ of fSAD and Norm have independent value when associated with lung function and emphysema, even when considering the amount of each (i.e., V^{fSAD}, V^{Norm}). Our approach for quantifying pocket formations of PRM^{fSAD} from normal lung parenchyma (PRM^{Norm}) may show promise as a CT readout of emphysema onset.

Keywords: chronic obstructive pulmonary disease; small airways disease; parametric response mapping; computed tomography of the chest; emphysema

1. Introduction

Chronic obstructive pulmonary disease (COPD) is a leading cause of death and healthcare burden in the United States and worldwide. Accounting for over 3 million deaths globally in 2015 ("Global, regional, and national deaths, prevalence, disability-adjusted life years, and years lived with disability for chronic obstructive pulmonary disease and asthma, 1990–2015," 2017), this disease is expected to rise in prevalence as the world population ages (Mannino & Buist, 2007). COPD is understood to be a complex heterogeneous disease presenting clinically diverse phenotypes (Barker & Brightling, 2013; Han et al., 2010). Major causes of airflow obstruction are attributed to chronic bronchiolitis, a.k.a small airways disease (SAD), and emphysema. Although SAD and emphysema are treated as separate COPD subtypes, studies have shown strong quantitative evidence that SAD exists as an intermediate state between healthy lung tissue and emphysema—i.e., irreversible lung damage—in COPD pathogenesis (Jennifer L. Boes et al., 2015; Labaki et al., 2019; McDonough et al., 2011). At present, little has been done to better quantify the onset of SAD from healthy lung parenchyma.

The Parametric Response Map (PRM) is a CT-based voxel-wise computational technique that can identify and quantify functional small airways disease (fSAD; indirect measure of SAD) even in the presence of emphysema (Galbán et al., 2012). The percent volume of PRM-derived fSAD (PRM^{fSAD}), i.e., the amount of fSAD in the lungs, has improved COPD phenotyping and the prediction of spirometric decline in subjects at risk of COPD (Bhatt et al., 2016). To determine the value of spatial features from each PRM classification, we developed topological PRM (tPRM) as an extension of the PRM algorithm (Hoff et al., 2017). These radiographic tPRM readouts were shown to improve upon commonly used whole-lung PRM measures with respect to COPD characterization, and correlate to structural changes in lung tissue samples from subjects diagnosed with bronchiolitis obliterans (Ram et al., 2022). Of interest is the Euler-Poincaré Characteristic (χ); positive values of this topological feature are associated with the

formation of pockets of like tissue (e.g., pockets of fSAD) (Hoff et al., 2017). χ, when generated from PRM^{fSAD} (χ^{fSAD}), may serve to detect lung parenchymal transition from healthy to emphysema through SAD.

The transition from normal parenchyma to SAD, and the relationship of this transition to emphysema, is the focus of this study. We investigated χ^{fSAD} as an index of COPD severity in baseline (Phase 1) data from COPDGene (Regan et al., 2011) and demonstrated the utility of our methodology to assess disease phenotype and transition of fSAD from normal lung parenchyma.

2. Materials and Methods

2.1 Study Sample

Our study was a secondary analysis of data from COPDGene (ClinicalTrials.gov: NCT00608764), a large Health Insurance Portability and Accountability Act-compliant prospective multi-center observational study. In Phase 1 (2007-2012), written and informed consent was obtained from all participants and the study was approved by local institutional review boards of all 21 centers. Ever-smokers with greater than or equal to 10 pack-year smoking history, with and without airflow obstruction, were enrolled between January 2008 and June 2011. Participants were non-Hispanic white or African American. Participants underwent volumetric inspiratory and expiratory CT using standardized protocol; images were transferred to a central lab for protocol verification and quality control (QC) (Regan et al., 2011). Exclusion criteria included a history of other lung disease (except asthma), prior surgical excision involving a lung lobe or greater, present cancer, metal in the chest, or history of chest radiation therapy. Participants were excluded from the present study due to inadequate CT for computing tPRM, such as missing an inspiration/expiration scan, or failing QC implemented specifically for the present study. Our QC protocol is described in the **Supplemental Methods**. Data for participants evaluated here have been utilized in numerous previous studies and a list of COPDGene publications can be found at http://www.copdgene.org/publications. Our study is the first to report tPRM analysis across the whole Phase 1 cohort of COPDGene participants.

Spirometry was performed in the COPDGene study before and after the administration of a bronchodilator, specifically 180 mcg of albuterol (Easy-One spirometer; NDD, Andover, MA). Post-bronchodilator values were used in our analyses. COPD was defined by a post-bronchodilator FEV_1/FVC of less than 0.7 at the baseline visit, as specified in the Global Initiative for Chronic Obstructive Lung Disease (GOLD) guidelines (Rabe et al., 2007). GOLD grades 1-4 were used to define disease severity. GOLD 0 classification, i.e., "at-risk," was

defined by a post-bronchodilator $FEV_1/FVC \geq 0.7$ at the baseline visit, alongside $FEV_1\%$ predicted ≥ 80%. Participants with $FEV_1/FVC \geq 0.7$ with $FEV_1\%$ predicted less than 80% were classified as having preserved ratio impaired spirometry (PRISm) (Wan et al., 2014). Demographic and spirometric measures used in this study included age, sex, race, smoking history, scanner manufacturer, body mass index (BMI), $FEV_1\%$ predicted, FEV_1/FVC and forced mid-expiratory flow (FEF_{25-75}).

2.2 Computed Tomography and Topological PRM Analysis

All computed tomography (CT) data were obtained from multiple sites associated with the COPDGene project. Whole-lung volumetric multidetector CT acquisition was performed at full inspiration and normal expiration using a standardized previously published protocol (Regan et al., 2011). Data reconstructed with the standard reconstruction kernel was used for quantitative analysis. All CT data were presented in Hounsfield units (HU), where stability of CT measurement for each scanner was monitored monthly using a custom COPDGene phantom (Regan et al., 2011). For reference, air and water attenuation values are −1,000 and 0 HU, respectively.

PRM were determined from paired CT scans using Lung Density Analysis (LDA) software (Imbio, LLC, Minneapolis, MN). LDA segmented the lungs from the thoracic cavity with airways removed. Inspiratory CT scans were spatially aligned to the expiratory geometric frame using deformable image registration. Lung voxels were classified using pre-determined HU thresholds as: normal (PRM^{Norm}, -950 < inspiration HU ≤ -810, and expiration HU ≥ -856), functional small airways disease (PRM^{fSAD}, -950 < inspiration HU ≤ -810, expiration HU < -856), emphysema (PRM^{Emph}, inspiration HU < -950, expiration HU < -856), or parenchymal disease (PRM^{PD}, inspiration HU > -810) (Belloli et al., 2016). Only voxels between -1,000 HU and -250 HU at both inspiration and expiration were used for PRM classification. Each PRM classification was quantified as the percent volume, which is defined as the sum of a PRM classification normalized to the total lung volume at expiration times 100.

Topological analysis of PRM was performed using methods previously described (Hoff et al., 2017). tPRM metrics were defined through application of Minkowski measures on 3D binary voxel distributions: volume density (V) and Euler-Poincaré Characteristic (χ) (Legland et al., 2007). Maps of V and χ were computed for each PRM class (Norm, fSAD, Emph and PD) using a moving window of size 21^3 voxels evaluated on a grid of every 5th voxel. V was normalized by the Minkowski estimate of the mask within the same local window volume (rather than a direct calculation of the mask volume in the window as previously described) and χ by the masked window voxel count. Linear interpolation was applied to determine V and χ values for all segmented voxels.

To indicate the PRM class associated with a Minkowski measure, the class is presented as a superscript (e.g., V^{fSAD} is the volume density of PRM^{fSAD}). tPRM analysis was performed using open-source and in-house software developed in MATLAB R2019a (MATLAB, The MathWorks Inc., Natick, MA). A detailed overview and diagram, of computing tPRM from raw imaging data, was made by Hoff et al. (Hoff et al., 2017). Because the focus of this study is on the relation between normal parenchyma to SAD, and its association with emphysema, all analyses were performed using V and χ for PRM classifications Norm and fSAD. For completeness, V and χ for PRM classifications Emph and PD are provided.

2.3 Statistical Analysis

Data in this study are presented as mean and standard deviation unless stated otherwise. Correlation between V and χ for PRM classes Norm and fSAD were calculated using Spearman rank-order correlation coefficients (ρ). The total cohort was separated into two subsets based on spirometry confirmed COPD: non-COPD ($FEV_1/FVC \geq 0.7$) and COPD ($FEV_1/FVC < 0.7$). Multivariable regression analysis was performed on both subsets using a stepwise approach with V and χ for PRM classifications Norm and fSAD as independent variables and selected

pulmonary function testing and clinical features as outcome variables, controlling for age, gender, race, BMI, smoking (pack years) and CT vendor. These control variables were included as compulsory independent variables in all regression models. Statistical work was conducted using IBM SPSS Statistics v27 (SPSS Software Products). In all tests significance was defined by $p < 0.05$.

2.4 Case Study: Spatial Analysis

In a single subject, we evaluated the relationship between V and χ for PRM^{fSAD} and PRM^{Emph}. The case is a female subject (46-50 years old) diagnosed with GOLD 4 COPD. First, a binary segmentation map was generated to identify lung regions with $V^{Emph} > 0.6$. Based on the binary map and visual inspection, a profile was determined from a lung region with $V^{Emph} > 0.6$ to $V^{Emph} < 0.2$ on a single axial slice. A line plot was produced for V and χ vs distance along each point of the profile. The distance, in units of cm, along the image profile was determined using the voxel dimensions of the CT scan.

3. Results

3.1 Population Characteristics

The original COPDGene Phase 1 cohort consisted of 10,300 individuals. We excluded 1,344 participants for: inadequate CT data, such as missing an expiration or inspiration scan, to conduct tPRM analysis (n = 1,125); missing clinical data (n = 16); or failing to pass our CT-based QC testing (n = 203). Further details of CT QC are provided in **Supplemental Methods**. The resulting complete subset used for analyses thus consisted of 8,956 participants. Baseline demographics and lung function for all participants, grouped based on FEV_1% predicted and FEV_1/FVC—that is, by GOLD grade or PRISm as described in the Materials and Methods—are reported in **Table 1**. There was a notably high proportion of GOLD 0 (FEV_1/FVC ≥ 0.7, FEV_1% predicted ≥ 80%) participants, accounting for almost half of the study population (43%; 3,867 of 8,956 participants). Increasing percent volume of PRM-derived fSAD (PRM^{fSAD}) and PRM-derived emphysema (PRM^{Emph}), with decreasing PRM^{Norm}, was observed with higher GOLD grades. This is consistent with previously published work. PRM-derived parenchymal disease (PRM^{PD}) was found to be elevated in PRISm and GOLD 0 participants (35.8 ± 16.4 and 26.3 ± 12.8% of the total lung volume, respectively) as compared to the COPD subset.

Table 1: **Clinical Characterization of the Study Population**

	Non-COPD		COPD			
Variable	GOLD 0	PRISm	GOLD 1	GOLD 2	GOLD 3	GOLD 4
Participants (N)	3867	1088	699	1732	1041	529
Age (yrs)	56.7 (8.36)	57.1 (8.20)	61.6 (8.96)	62.6 (8.86)	64.3 (8.27)	64.1 (7.53)
Sex (M/F)	2048/1819	496/592	399/300	933/799	604/437	314/215
BMI (kg/cm^2)	29.0 (5.79)	31.9 (7.31)	27.1 (4.89)	28.7 (6.06)	28.1 (6.33)	25.3 (5.56)
Smoking Pack-Years	37.2 (20.0)	42.6 (24.2)	45.0 (24.4)	50.9 (26.8)	55.1 (27.1)	56.7 (28.7)
FEV_1% Predicted (%)	97.4 (11.4)	70.6 (7.89)	90.8 (8.70)	65.0 (8.51)	40.2 (5.69)	22.6 (4.84)
FEV_1/FVC	0.79 (0.05)	0.77 (0.05)	0.65 (0.04)	0.58 (0.08)	0.44 (0.09)	0.31 (0.07)
FEF_{25-75}(L/s)	2.81 (1.00)	1.79 (0.66)	1.31 (0.50)	0.80 (0.35)	0.39 (0.16)	0.21 (0.08)
PRM^{Norm}(%)	61.7 (13.0)	53.8 (14.6)	56.9 (12.1)	49.1 (13.5)	33.0 (12.5)	21.1 (9.13)
PRM^{fSAD}(%)	9.90 (9.31)	8.88 (8.25)	17.0 (10.8)	21.3 (11.5)	30.9 (11.0)	36.0 (8.94)
PRM^{Emph}(%)	0.80 (1.42)	0.73 (2.29)	3.00 (3.49)	5.40 (6.95)	14.7 (12.2)	26.0 (14.0)
PRM^{PD}(%)	26.3 (12.8)	35.8 (16.4)	20.8 (8.44)	22.2 (9.04)	19.6 (9.29)	15.7 (5.43)

Notes: Participant characteristics of the entire study population separated in subsets of those with (FEV_1/FVC < 0.7) and without (FEV_1/FVC ≥ 0.7) COPD. Values are displayed as mean (standard deviation). GOLD, Global Initiative for Chronic Obstructive Lung Disease; PRISm, preserved ratio impaired spirometry; GOLD 0, at-risk smokers with normal spirometry; BMI, body mass index; FEV_1, forced expiratory volume in one second; FVC, forced vital capacity; FEF_{25-75}, forced mid-expiratory flow; PRM, parametric response map; Norm, Normal; fSAD, functional small airways disease; Emph, emphysema; PD, parenchymal disease.

3.2 Topological Readouts of PRM

Presented in **Figure 1** is a case with elevated fSAD (PRM^{fSAD} = 40%). Representative coronal slices of the expiration CT scan and PRM^{fSAD}, overlayed on CT scan, are provided. To illustrate the dependence of V and χ on the arrangement of PRM^{fSAD}, we have included V^{fSAD} and χ^{fSAD} maps indicating regions with low (cyan box) and high (magenta box) V^{fSAD}. As expected, V^{fSAD} (**Figure 1C**) is dependent on the amount of fSAD (yellow voxels in **Figure 1B**). Averaged over the lungs, V^{fSAD} is proportional to the percent volume of PRM^{fSAD} by a factor of 100.

However, $\chi^{fSAD} > 0$ (cyan box in **Figure 1D**) corresponds to the formation of fSAD pockets (cyan box **Figure 1B**), whereas $\chi^{fSAD} < 0$ (cyan box in **Figure 1D**) is the consolidation of these pockets into a mesh with holes (magenta box in **Figure 1B**).

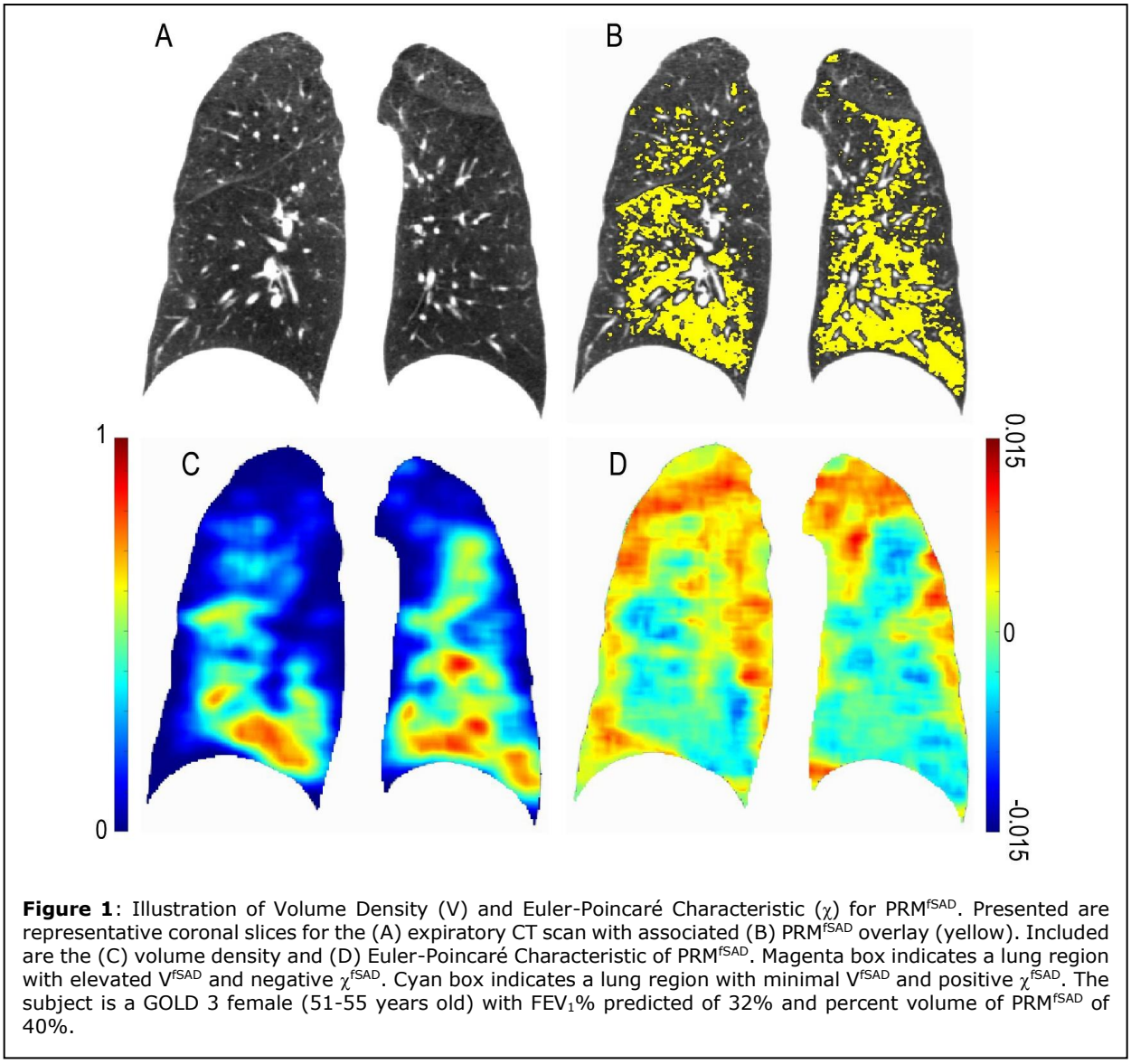

Figure 1: Illustration of Volume Density (V) and Euler-Poincaré Characteristic (χ) for PRM^{fSAD}. Presented are representative coronal slices for the (A) expiratory CT scan with associated (B) PRM^{fSAD} overlay (yellow). Included are the (C) volume density and (D) Euler-Poincaré Characteristic of PRM^{fSAD}. Magenta box indicates a lung region with elevated V^{fSAD} and negative χ^{fSAD}. Cyan box indicates a lung region with minimal V^{fSAD} and positive χ^{fSAD}. The subject is a GOLD 3 female (51-55 years old) with FEV_1% predicted of 32% and percent volume of PRM^{fSAD} of 40%.

The volume density of PRM^{Norm} and PRM^{fSAD} demonstrated an inverse relationship with increasing COPD severity (**Figure 2A**), consistent with previous work. A similar inverse relationship was observed for χ of both normal lung and fSAD (χ^{Norm} and χ^{fSAD}). Values of χ^{Norm} and χ^{fSAD} were found to flip about zero (e.g., χ^{fSAD} changes from positive to negative values) from GOLD 2 to GOLD 4 (**Figure 2B**). As provided in **Supplemental Table 1**, χ^{Norm} and χ^{fSAD}

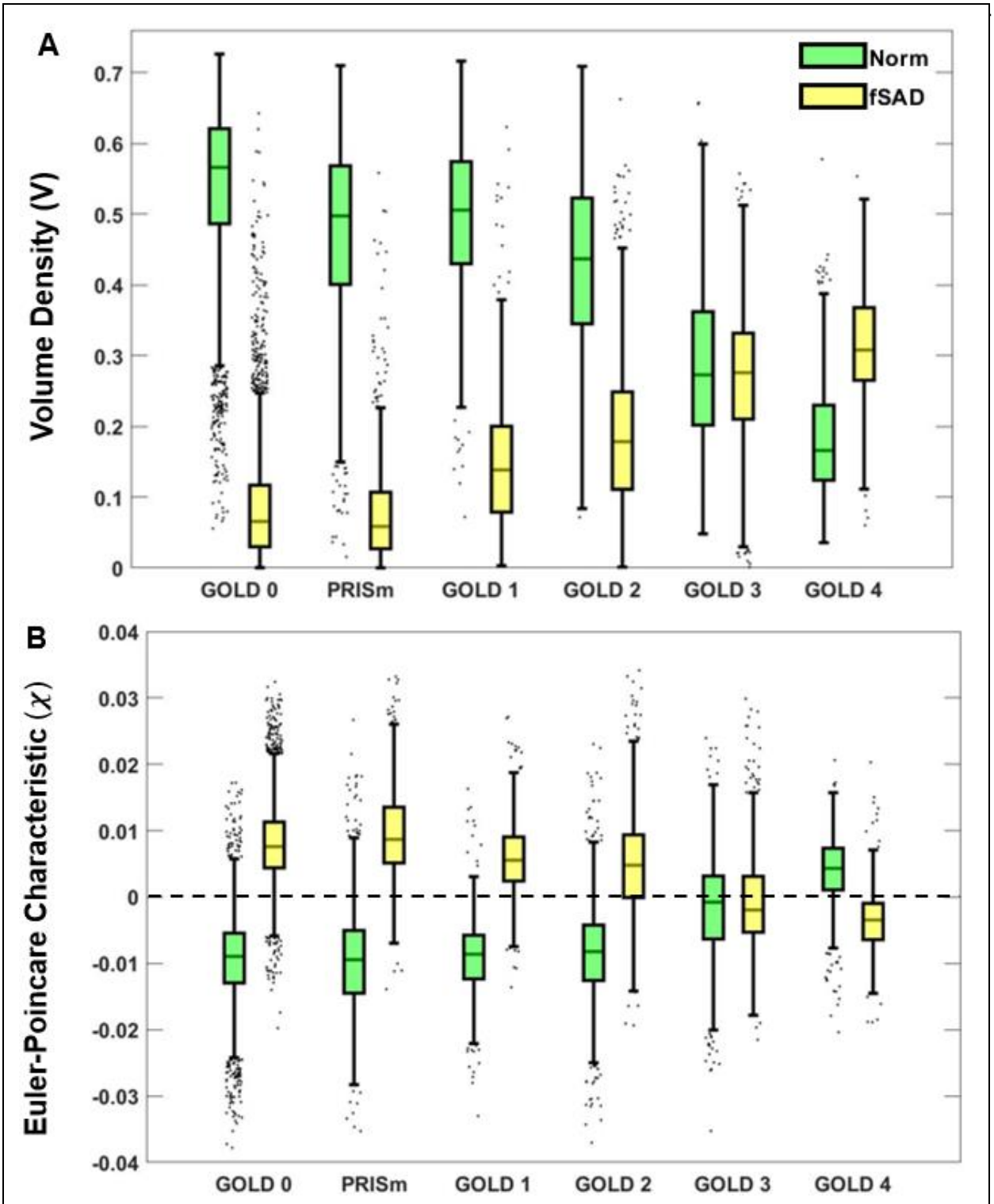

Figure 2: Boxplots for Volume Density (V) and Euler-Poincaré Characteristic (χ) of PRM^{Norm} and PRM^{fSAD} across all GOLD stages, "at-risk" (GOLD 0) and PRISm. Plots of (A) V and (B) χ are provided for PRM^{Norm} (green) and PRM^{fSAD} (yellow). Box plots were computed following standard protocol for box and whiskers. Box lines determined by lower quartile (Q1), middle quartile / median (Q2), and upper quartile (Q3). Whiskers are drawn out to Q1 - 1.5 x IQR and Q3 + 1.5 x IQR for lower and upper limits respectively. IQR = Q3-Q1. Outliers are defined as points beyond the given upper and lower limits and illustrated as black points with a random bounded horizontal perturbation beyond box whiskers.

cases diagnosed as GOLD 2. For those with severe COPD, i.e., GOLD 4, χ^{Norm} and χ^{fSAD} were 0.0039 (0.0055) and -0.0036 (0.0048), respectively. Mean values of χ^{Emph} and χ^{PD} were found to be positive and similar across GOLD status (**Supplemental Table 1**).

We further evaluated the relationship of PRM^{Norm} and PRM^{fSAD} with respect to V (**Figure 3A**) and χ (**Figure 3B**). Both V and χ demonstrated strong correlations between Norm and fSAD (ρ = -0.666, $p < 0.001$ and ρ = -0.745, $p < 0.001$, respectively) over the full study cohort. Here the GOLD stage is represented by different colors and the relative amount of emphysema, quantified by V^{Emph}, by size of the bubbles. As observed in **Figure 3A**, V^{Norm} versus V^{fSAD} had more scatter in the data compared to χ^{Norm} versus χ^{fSAD} (**Figure 3B**). Cases with elevated emphysema (V^{Emph}) demonstrated lower V^{fSAD} and $\chi^{Norm} > 0$, but demonstrated positive and negative values of χ^{fSAD} (**Figure 3B**).

3.3 Multivariable Regression Analysis

Presented in **Table 2** are results from multivariable regression analyses that demonstrate the contribution of V and χ for Norm and fSAD when modeling spirometric measures and the volume density of emphysema, controlling for age, sex, race, BMI, pack-years and CT vendor. Among those with spirometrically confirmed COPD, V^{Norm} was found to be significantly associated with multiple clinical outcomes including FEV_1% predicted, FEV_1/FVC, FEF_{25-75} and V^{Emph} (see **Table 2**). V^{fSAD} and χ^{fSAD} were found to independently contribute significantly to FEV_1% predicted (β = 0.065, p=0.004 and β = 0.106, p<0.001). Only the Norm measures were found to contribute to FEV_1/FVC (β = 0.668, p<0.001 for V^{Norm} and β = -0.120, p<0.001 for χ^{Norm}), whereas V and χ for both Norm and fSAD were found to be significant parameters for FEF_{25-75}. With respect to V^{Emph}, extent of emphysema, V and χ for Norm and fSAD were highly significant but demonstrated similar trends irrespective of PRM classification. For completeness, the same analyses were performed on the non-COPD cohort (**Supplemental**

Table 2). As compared to the COPD cohort, statistical models generated from the non-COPD cohort demonstrate weaker correlations (i.e., adjusted R^2) with significant parameters.

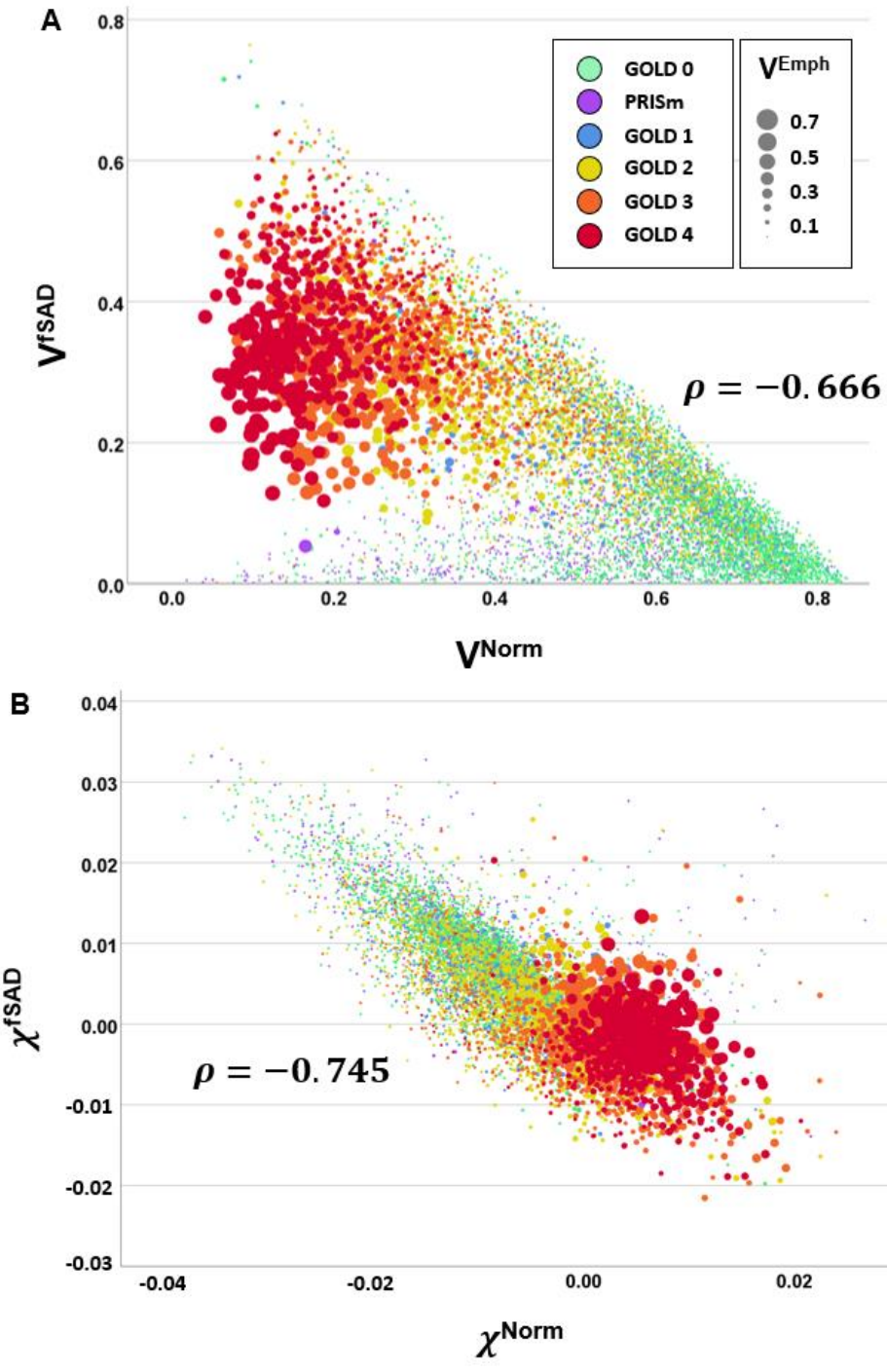

Figure 3: Scatter plots of all study sample participants for (A) V^{Norm} versus V^{fSAD} and (B) χ^{Norm} versus χ^{fSAD}. Individual points are color coded based on COPD classifications. The size of the points indicates the amount of emphysema as measured by the volume density of PRM^{Emph} (V^{Emph}).

Table 2: Multivariable Regression for COPD Subset

Performance	FEV_1% predicted	FEV_1/FVC	FEF_{25-75} (L)	V^{Emph}
Adjusted R^2	0.516	0.602	0.526	0.778
SE	15.8	0.084	0.331	0.057
Age (yrs)	0.085**	0.021 (0.06)	-0.184**	0.035**
Sex (M/F)		0.018 (0.08)	-0.283**	-0.035**
BMI (kg/cm^2)	-0.110**	0.033*		-0.232**
Smoking Pack Years	-0.046**	-0.013 (0.22)	-0.051**	-0.015 (0.06)
CT vendor				0.111**
Race		0.113**	-0.033*	
V^{Norm}	0.727**	0.668**	0.688**	-1.01**
V^{fSAD}	0.065*		0.138**	-0.408**
χ^{Norm}		-0.120**	0.134**	0.150**
χ^{fSAD}	0.106**		0.175**	0.118**

Notes: Multivariable regression modelling using volume density (V) and Euler-Poincaré Characteristic (χ) for PRM-derived Normal and fSAD (introduced stepwise) to model pulmonary function testing measures in the COPD subset. Each column presents results for a different regression model. FEV_1, forced expiratory volume in one second; FVC, forced vital capacity; FEF_{25-75}, forced mid-expiratory flow; Emph, emphysema; SE, standard error of the estimate; BMI, body mass index; Norm, Normal; fSAD, functional small airways disease. Model performance is reported as adjusted R^2 and standard error of the estimate. Feature association is reported as standardized beta coefficients (β); cells for stepwise variables removed from final model. All regression models were controlled for age, sex, race, BMI, pack years and CT vendor. P values ≥ 0.01, < 0.01 and ≥ 0.001, and < 0.001 are presented as values in parentheses, *, and **, respectively.

3.4 Dependence Between Topologies of PRM^{fSAD} and PRM^{Emph}

As expected from the multivariable analysis, V^{fSAD} was strongly correlated to V^{Emph} ($r = 0.845$, $p < 0.001$). Nevertheless, only a weak correlation was observed between χ^{fSAD} and χ^{Emph} ($\rho = -0.155$, $p < 0.001$). As the topologies of PRM were determined as averages over the whole lungs, we provide a case study illustrating the relationship between V and χ of PRM^{fSAD} and PRM^{Emph} at the local level. Presented in **Figure 4** are the profiles of V and χ of PRM^{fSAD} and

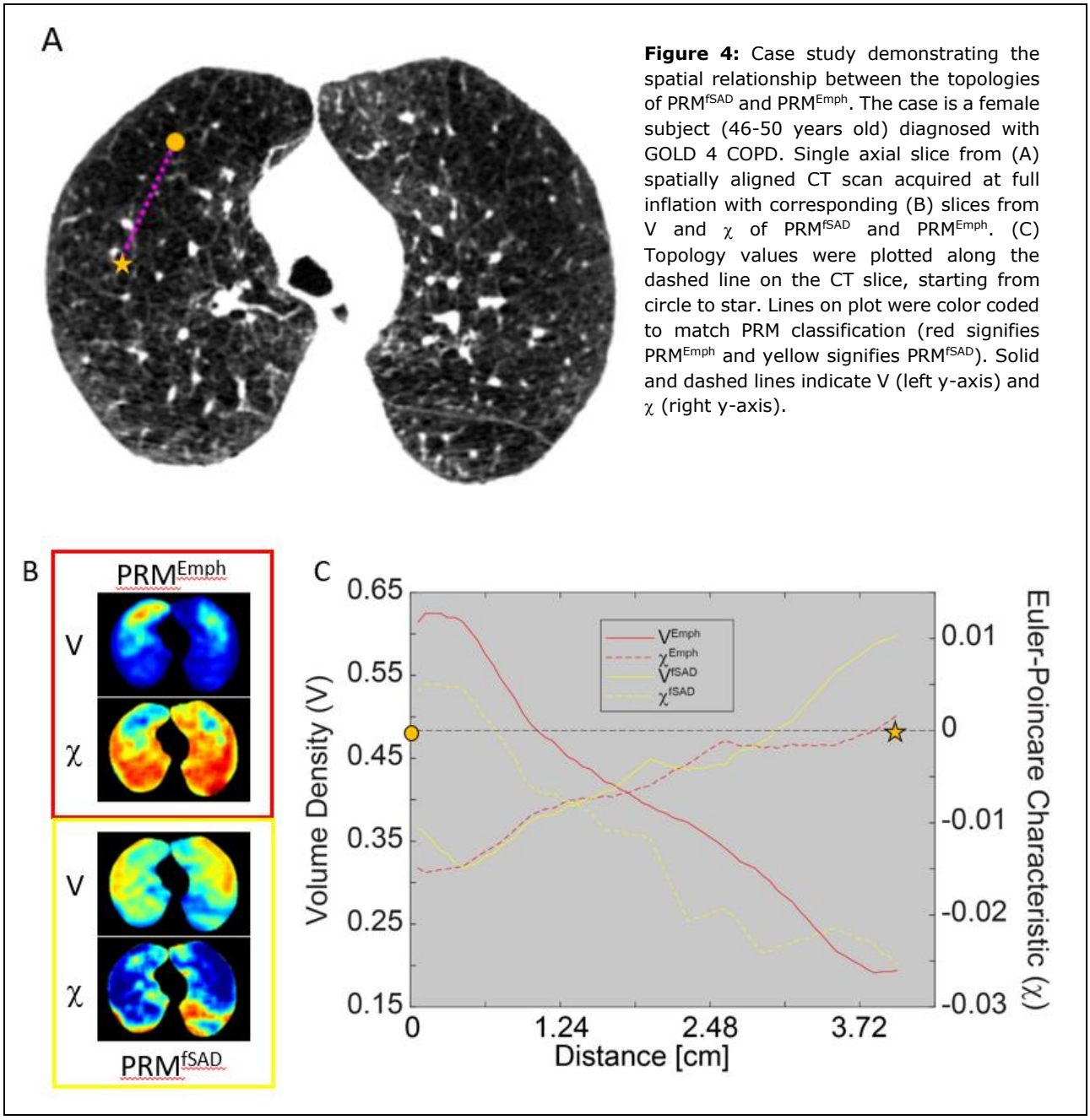

Figure 4: Case study demonstrating the spatial relationship between the topologies of PRM^{fSAD} and PRM^{Emph}. The case is a female subject (46-50 years old) diagnosed with GOLD 4 COPD. Single axial slice from (A) spatially aligned CT scan acquired at full inflation with corresponding (B) slices from V and χ of PRM^{fSAD} and PRM^{Emph}. (C) Topology values were plotted along the dashed line on the CT slice, starting from circle to star. Lines on plot were color coded to match PRM classification (red signifies PRM^{Emph} and yellow signifies PRM^{fSAD}). Solid and dashed lines indicate V (left y-axis) and χ (right y-axis).

PRM^{Emph} from a region of the right lung with elevated and reduced V^{Emph} (orange circle and star, respectively, in **Figure 4A** and **C**). The case is a female subject (46-50 years old) diagnosed with GOLD 4 COPD. The subject was found to have over the lungs high levels of V^{fSAD} (0.37) with relatively elevated V^{Emph} (0.1). Mean values of χ were 0.008 and -0.009 for PRM^{Emph} and PRM^{fSAD}, respectively. As seen in **Figure 4C**, V^{fSAD} increased while V^{Emph} decreased further from lung with the highest level of V^{Emph} (~0.6 at orange circle in **Figure 4A** and **C**). At approximately 1.8cm, volume densities between PRM^{fSAD} and PRM^{Emph} transitioned. Inversely, χ^{fSAD} was found to increase with decreasing χ^{Emph} with transition occurring at ~1.2cm.

4. Discussion

The topological parametric response map is an extension of the well-established PRM method, a powerful quantitative imaging marker (Galbán et al., 2012). In this study, we have demonstrated that inclusion of topological features, in this case the Euler-Poincaré Characteristic (χ), improved characterization and interpretation of fSAD in COPD as a complimentary readout of volume density (V), which is equivalent to traditional percent volume of PRM classifications (Hoff et al., 2017). This study also evaluated the role of PRM-defined normal parenchyma (PRM^{Norm}) and fSAD (PRM^{fSAD}) as lone indicators of COPD severity. We observed distinct patterns in topological metrics with respect to GOLD grades and identified a complete inversion in topology, characterized by Euler-Poincaré Characteristic χ, between normal lung and fSAD, in mid-to-late stages of COPD. We also found statistically significant associations of spirometric measures and emphysema with V and χ of PRM^{Norm} and PRM^{fSAD}.

Our study builds on previous work by Hoff et al (Hoff et al., 2017) on tPRM characterization in COPD. This study used a much smaller population (n = 88) to demonstrate the trends of all four topological features (volume density, surface area, mean curvature and Euler-Poincaré Characteristic) with increasing COPD severity (Hoff et al., 2017). Limited in statistical power, it instead focused on the surface area of fSAD. Access to a notably larger population (n = 8,956) allowed us in the current study to evaluate the volume density (V) and Euler-Poincaré Characteristic (χ) of PRM^{Norm} and PRM^{fSAD} and relate our findings to the field's current understanding of COPD progression; i.e., normal parenchyma transitions to emphysema through SAD.

A key finding of this study is the ability to quantify parenchymal lung health, based not only on the extent but also on the arrangement of local lung abnormalities, i.e., fSAD. This is rooted in the concept that the lungs are healthy (i.e., PRM^{Norm}) and COPD progresses through SAD (i.e., PRM^{fSAD}), which is an intermediate between normal and emphysematous lung

tissue. The nature of this transition suggests χ may be capturing a fundamental mechanism in the emergence of fSAD. Based on our observation, fSAD appears to develop as distinct pockets within healthy lung tissue as depicted in cyan box in **Figure 1B**. With increasing COPD severity, fSAD pockets coalesce to a mesh, which is represented by decreasing values in χ^{fSAD} (magenta box in **Figure 1B**). On a whole lung level, this transition occurs on average from GOLD stages 2 to 4. By quantifying the amount and arrangement of normal and fSAD parenchyma, one can obtain a full assessment of the COPD lung. As fSAD is an intermediate between healthy lung and emphysema, increasing levels of emphysema have a direct effect on V and χ of fSAD. This is observed in **Figure 3**, where increasing values of V^{Emph} resulted in a drop in V^{fSAD} and increase in χ^{fSAD}. These trends were reflected in our multivariable model for V^{Emph} as well (**Table 2**).

We postulate that the transition observed between χ^{Norm} and χ^{fSAD} (**Figures 2** and **3**) should be observed for χ^{fSAD} and χ^{Emph}. Using mean values of χ over the lungs, χ^{Emph} was found to be relatively stable, generating positive values across GOLD (**Supplemental Table 2**). In a recent study, Bhatt and colleagues evaluated a CT readout, referred to as the mean Jacobian determinant of normal voxels, at varying distances from emphysematous tissue (Bhatt et al., 2017). When measured at a distance of 2mm from CT voxels designated emphysema (i.e., voxel HU <-950HU), this CT-based readout was found to be predictive of spirometric decline. We applied a similar strategy to determine if a relationship between χ^{fSAD} and χ^{Emph} is observed at the local level (**Figure 4**). Our spatial analysis of a single case clearly demonstrates a transition in topologies of PRM^{fSAD} and PRM^{Emph}. Although the readouts reported by Bhatt and colleagues lacked quantification of SAD, there is clear agreement that lung tissue along the periphery of emphysematous tissue provides potential insight into COPD progression. Additional evidence is from the seminal work by McDonough and colleagues (McDonough et al., 2011). In this study they provided pathological evidence demonstrating the role of SAD in COPD progression. Using high resolution (~10 μm) microCT to analyze frozen lung samples

from lung transplant recipients with end-stage COPD, they found that widespread narrowing and destruction of the smaller airways (i.e., SAD) occurred before emphysematous lesions became large enough to be visible on standard CT imaging. They concluded that SAD might serve as an emphysema precursor. We suspect that the transition of χ^{fSAD} and χ^{Emph} may be capturing what was observed using microCT of lung explants.

We acknowledge several notable limitations. COPDGene comprises over 20 study sites, making scanner variation and reconstruction kernel inconsistency inevitable. Sensitivity of PRM to scanner variability was addressed previously, and although effort was made to apply PRM only to soft kernels, variability in scanner type was unavoidable. However, we included scanner vendor in our multivariable regressions and found that it did not significantly confound models. Another limitation is variation in levels of inspiration and expiration during CT acquisition. Earlier work demonstrated that even small perturbations from functional residual capacity (FRC) have an observable effect on threshold-based techniques such as PRM (J. L. Boes et al., 2015). To limit this, we implemented QC that excluded participants based on erroneous volume changes or strong discordance with correlation between PRM^{Norm} and FEV_1% predicted.

5. Conclusions

In summary, we have demonstrated that topological features, V and χ, are able to enhance the sensitivity of PRM classifications, notably Norm and fSAD, to COPD severity. This data supports the concept that as pockets of small airways disease coalesce, surrounding normal tissue is lost. These pockets of fSAD are correlated with increasing presence of emphysema, independent of the amount of fSAD present. We further demonstrated at the local level that χ^{fSAD} and χ^{Emph} correlate, which may be explained by McDonough and colleagues' observations using microCT. Our study provides a unique strategy to detect subtle changes in lung parenchyma that may progress to emphysema. This approach to monitoring extent and arrangement of Norm and fSAD may offer insight into COPD phenotypes and provide

prognostic information that has relevance in clinical care and future clinical trials. Better computational strategies must be developed before these topologies can be used to detect local emphysema onset.

Funding

This work was supported by the National Heart, Lung, and Blood Institute of the National Institutes of Health Grants R01 HL139690 and R01 HL150023 and by the National Heart, Lung, and Blood Institute of the National Institutes of Health Grants U01 HL089897 and U01 HL089856, which support the COPDGene study. The COPDGene study (NCT00608764) is also supported by the COPD Foundation through contributions made to an Industry Advisory Committee comprised of AstraZeneca, Bayer Pharmaceuticals, Boehringer-Ingelheim, Genentech, GlaxoSmithKline, Novartis, Pfizer and Sunovion.

Conflict of Interest Statement

W.W.L. reports personal fees from Konica Minolta and Continuing Education Alliance. B.A.H. and C.J.G. are co-inventors and patent holders of tPRM, which the University of Michigan has licensed to Imbio, LLC. C.J.G. is co-inventor and patent holder of PRM, which the University of Michigan has licensed to Imbio, LLC. B.A.H. and C.J.G. have financial interest in Imbio, LLC. C.R.H. is employed by Imbio, LLC. D.A.L. reports funds paid to the institution from the NIH, and Boehringer Ingelheim. M.K.H. reports personal fees from GlaxoSmithKline, AstraZeneca, Boehringer Ingelheim, Cipla, Chiesi, Novartis, Pulmonx, Teva, Verona, Merck, Mylan, Sanofi, DevPro, Aerogen, Polarian, Regeneron, Amgen, UpToDate, Altesa Biopharma, Medscape, NACE, MDBriefcase and Integrity. She has received either in kind research support or funds paid to the institution from the NIH, Novartis, Sunovion, Nuvaira, Sanofi, AstraZeneca, Boehringer Ingelheim, Gala Therapeutics, Biodesix, the COPD Foundation and the American Lung Association. She has participated in Data Safety Monitoring Boards for Novartis and Medtronic with funds paid to the institution. She has received stock options from Meissa Vaccines and Altesa Biopharma. For the remaining authors none were declared.

Acknowledgements

We acknowledge the COPDGene investigators for their role in the study providing data for this project:

Administrative Center: James D. Crapo, MD (PI); Edwin K. Silverman, MD, PhD (PI); Barry J. Make, MD; Elizabeth A. Regan, MD, PhD

Genetic Analysis Center: Terri Beaty, PhD; Ferdouse Begum, PhD; Peter J. Castaldi, MD, MSc; Michael Cho, MD; Dawn L. DeMeo, MD, MPH; Adel R. Boueiz, MD; Marilyn G. Foreman, MD, MS; Eitan Halper-Stromberg; Lystra P. Hayden, MD, MMSc; Craig P. Hersh, MD, MPH; Jacqueline Hetmanski, MS, MPH; Brian D. Hobbs, MD; John E. Hokanson, MPH, PhD; Nan Laird, PhD; Christoph Lange, PhD; Sharon M. Lutz, PhD; Merry-Lynn McDonald, PhD; Margaret M. Parker, PhD; Dmitry Prokopenko, Ph.D; Dandi Qiao, PhD; Elizabeth A. Regan, MD, PhD; Phuwanat Sakornsakolpat, MD; Edwin K. Silverman, MD, PhD; Emily S. Wan, MD; Sungho Won, PhD

Imaging Center: Juan Pablo Centeno; Jean-Paul Charbonnier, PhD; Harvey O. Coxson, PhD; Craig J. Galban, PhD; MeiLan K. Han, MD, MS; Eric A. Hoffman, Stephen Humphries, PhD; Francine L. Jacobson, MD, MPH; Philip F. Judy, PhD; Ella A. Kazerooni, MD; Alex Kluiber; David A. Lynch, MB; Pietro Nardelli, PhD; John D. Newell, Jr., MD; Aleena Notary; Andrea Oh, MD; Elizabeth A. Regan, MD, PhD; James C. Ross, PhD; Raul San Jose Estepar, PhD; Joyce Schroeder, MD; Jered Sieren; Berend C. Stoel, PhD; Juerg Tschirren, PhD; Edwin Van Beek, MD, PhD; Bram van Ginneken, PhD; Eva van Rikxoort, PhD; Gonzalo Vegas Sanchez-Ferrero, PhD; Lucas Veitel; George R. Washko, MD; Carla G. Wilson, MS;

PFT QA Center, Salt Lake City, UT: Robert Jensen, PhD

Data Coordinating Center and Biostatistics, National Jewish Health, Denver, CO: Douglas Everett, PhD; Jim Crooks, PhD; Katherine Pratte, PhD; Matt Strand, PhD; Carla G. Wilson, MS

Epidemiology Core, University of Colorado Anschutz Medical Campus, Aurora, CO: John E. Hokanson, MPH, PhD; Gregory Kinney, MPH, PhD; Sharon M. Lutz, PhD; Kendra A. Young, PhD

Mortality Adjudication Core: Surya P. Bhatt, MD; Jessica Bon, MD; Alejandro A. Diaz, MD, MPH; MeiLan K. Han, MD, MS; Barry Make, MD; Susan Murray, ScD; Elizabeth Regan, MD; Xavier Soler, MD; Carla G. Wilson, MS

Biomarker Core: Russell P. Bowler, MD, PhD; Katerina Kechris, PhD; Farnoush Banaei-Kashani, Ph.D

We would also like to acknowledge our copy editor Lee Olsen for her assistance in preparing this manuscript.

References

Barker, B. L., & Brightling, C. E. (2013). Phenotyping the heterogeneity of chronic obstructive pulmonary disease. *Clin Sci (Lond)*, *124*(6), 371-387. https://doi.org/10.1042/CS20120340

Belloli, E. A., Degtiar, I., Wang, X., Yanik, G. A., Stuckey, L. J., Verleden, S. E., Kazerooni, E. A., Ross, B. D., Murray, S., Galbán, C. J., & Lama, V. N. (2016). Parametric Response Mapping as an Imaging Biomarker in Lung Transplant Recipients. *American Journal of Respiratory and Critical Care Medicine*, *195*(7), 942-952. https://doi.org/10.1164/rccm.201604-0732OC

Bhatt, S. P., Bodduluri, S., Hoffman, E. A., John D. Newell, J., Sieren, J. C., Dransfield, M. T., & Reinhardt, J. M. (2017). Computed Tomography Measure of Lung at Risk and Lung Function Decline in Chronic Obstructive Pulmonary Disease. *American Journal of Respiratory and Critical Care Medicine*, *196*(5), 569-576. https://doi.org/10.1164/rccm.201701-0050OC

Bhatt, S. P., Soler, X., Wang, X., Murray, S., Anzueto, A. R., Beaty, T. H., Boriek, A. M., Casaburi, R., Criner, G. J., Diaz, A. A., Dransfield, M. T., Curran-Everett, D., Galbán, C. J., Hoffman, E. A., Hogg, J. C., Kazerooni, E. A., Kim, V., Kinney, G. L., Lagstein, A., . . . Han, M. K. (2016). Association between Functional Small Airway Disease and FEV1 Decline in Chronic Obstructive Pulmonary Disease. *American Journal of Respiratory and Critical Care Medicine*, *194*(2), 178-184. https://doi.org/10.1164/rccm.201511-2219OC

Boes, J. L., Bule, M., Hoff, B. A., Chamberlain, R., Lynch, D. A., Stojanovska, J., Martinez, F. J., Han, M. K., Kazerooni, E. A., Ross, B. D., & Galban, C. J. (2015). The Impact of Sources of Variability on Parametric Response Mapping of Lung CT Scans. *Tomography*, *1*(1), 69-77. https://doi.org/10.18383/j.tom.2015.00148

Boes, J. L., Hoff, B. A., Bule, M., Johnson, T. D., Rehemtulla, A., Chamberlain, R., Hoffman, E. A., Kazerooni, E. A., Martinez, F. J., Han, M. K., Ross, B. D., & Galbán, C. J. (2015). Parametric Response Mapping Monitors Temporal Changes on Lung CT Scans in the Subpopulations and Intermediate Outcome Measures in COPD Study (SPIROMICS). *Academic Radiology*, *22*(2), 186-194. https://doi.org/10.1016/j.acra.2014.08.015

Galbán, C. J., Han, M. K., Boes, J. L., Chughtai, K. A., Meyer, C. R., Johnson, T. D., Galbán, S., Rehemtulla, A., Kazerooni, E. A., Martinez, F. J., & Ross, B. D. (2012). Computed tomography–based biomarker provides unique signature for diagnosis of COPD phenotypes and disease progression. *Nature Medicine*, *18*(11), 1711-1715. https://doi.org/10.1038/nm.2971

Global, regional, and national deaths, prevalence, disability-adjusted life years, and years lived with disability for chronic obstructive pulmonary disease and asthma, 1990–2015: a systematic analysis for the Global Burden of Disease Study 2015. (2017). *The Lancet. Respiratory Medicine*, *5*(9), 691-706. https://doi.org/10.1016/S2213-2600(17)30293-X

Han, M. K., Agusti, A., Calverley, P. M., Celli, B. R., Criner, G., Curtis, J. L., Fabbri, L. M., Goldin, J. G., Jones, P. W., MacNee, W., Make, B. J., Rabe, K. F., Rennard, S. I., Sciurba, F. C., Silverman, E. K., Vestbo, J., Washko, G. R., Wouters, E. F. M., & Martinez, F. J. (2010). Chronic Obstructive Pulmonary Disease Phenotypes. *American Journal of Respiratory and Critical Care Medicine*, *182*(5), 598-604. https://doi.org/10.1164/rccm.200912-1843CC

Hoff, B. A., Pompe, E., Galbán, S., Postma, D. S., Lammers, J.-W. J., ten Hacken, N. H. T., Koenderman, L., Johnson, T. D., Verleden, S. E., de Jong, P. A., Mohamed Hoesein, F. A. A., van den Berge, M., Ross, B. D., & Galbán, C. J. (2017). CT-Based Local Distribution Metric Improves Characterization of COPD. *Scientific Reports*, *7*(1), 2999. https://doi.org/10.1038/s41598-017-02871-1

Labaki, W. W., Gu, T., Murray, S., Hatt, C. R., Galban, C. J., Ross, B. D., Martinez, C. H., Curtis, J. L., Hoffman, E. A., Pompe, E., Lynch, D. A., Kazerooni, E. A., Martinez, F. J., & Han, M. K. (2019). Voxel-Wise Longitudinal Parametric Response Mapping Analysis of Chest Computed Tomography in Smokers. *Acad Radiol*, *26*(2), 217-223. https://doi.org/10.1016/j.acra.2018.05.024

Legland, D., Kiêu, K., & Devaux, M.-F. (2007). COMPUTATION OF MINKOWSKI MEASURES ON 2D AND 3D BINARY IMAGES. *Image Analysis & Stereology*, *26*(2), 83-92. https://doi.org/10.5566/ias.v26.p83-92

Mannino, D. M., & Buist, A. S. (2007). Global burden of COPD: risk factors, prevalence, and future trends. *The Lancet*, *370*(9589), 765-773. https://doi.org/10.1016/S0140-6736(07)61380-4

McDonough, J. E., Yuan, R., Suzuki, M., Seyednejad, N., Elliott, W. M., Sanchez, P. G., Wright, A. C., Gefter, W. B., Litzky, L., Coxson, H. O., Paré, P. D., Sin, D. D., Pierce, R. A., Woods, J. C., McWilliams, A. M., Mayo, J. R., Lam, S. C., Cooper, J. D., & Hogg, J. C. (2011). Small-Airway Obstruction and Emphysema in Chronic Obstructive Pulmonary Disease. *New England Journal of Medicine*, *365*(17), 1567-1575. https://doi.org/10.1056/NEJMoa1106955

Rabe, K. F., Hurd, S., Anzueto, A., Barnes, P. J., Buist, S. A., Calverley, P., Fukuchi, Y., Jenkins, C., Rodriguez-Roisin, R., van Weel, C., & Zielinski, J. (2007). Global Strategy for the Diagnosis, Management, and Prevention of Chronic Obstructive Pulmonary Disease. *American Journal of Respiratory and Critical Care Medicine*, *176*(6), 532-555. https://doi.org/10.1164/rccm.200703-456SO

Ram, S., Verleden, S. E., Bell, A. J., Hoff, B. A., Labaki, W. W., Murray, S., Vanaudenaerde, B. M., Vos, R., Verleden, G. M., Kazerooni, E. A., Galbán, S., Hatt, C. R., Han, M. K., Lama, V. N., & Galbán, C. J. (2022). Quantitative CT Correlates with Local Inflammation in Lung of Patients with Subtypes of Chronic Lung Allograft Dysfunction. *Cells*, *11*(4), 699. https://www.mdpi.com/2073-4409/11/4/699

Regan, E. A., Hokanson, J. E., Murphy, J. R., Make, B., Lynch, D. A., Beaty, T. H., Curran-Everett, D., Silverman, E. K., & Crapo, J. D. (2011). Genetic Epidemiology of COPD (COPDGene) Study Design. *COPD: Journal of Chronic Obstructive Pulmonary Disease*, *7*(1), 32-43. https://doi.org/10.3109/15412550903499522

Wan, E. S., Castaldi, P. J., Cho, M. H., Hokanson, J. E., Regan, E. A., Make, B. J., Beaty, T. H., Han, M. K., Curtis, J. L., Curran-Everett, D., Lynch, D. A., DeMeo, D. L., Crapo, J. D., Silverman, E. K., & Investigators, C. O. (2014). Epidemiology, genetics, and subtyping of preserved ratio impaired spirometry (PRISm) in COPDGene. *Respir Res*, *15*, 89. https://doi.org/10.1186/s12931-014-0089-y